Surface phonons in thin aluminum oxide films: Thickness, beam-energy, and symmetry-mixing effects

B. G. Frederick
Department of Chemistry, Cornell University, Ithaca, New York 14853

G. Apai*
Corporate Research Laboratories, Eastman Kodak Company, Rochester, New York 14650-2001

T. N. Rhodin
Department of Applied and Engineering Physics, Cornell University, Ithaca, New York 14853
(Received 3 October 1990; revised manuscript received 27 February 1991)

The surface-phonon (Fuchs-Kliewer) modes of thin α-Al_2O_3 films prepared on a Ru(001) substrate have been measured with high-resolution electron-energy-loss spectroscopy. An understanding of the differences in phonon spectra for thick cyrstals versus thin films is derived from calculations using dielectric theory and the infrared optical constants for α-Al_2O_3. In addition to the three characteristic phonon modes assigned previously at $\sim$400, $\sim$650, and $\sim$900 cm^{-1} for $\sim$10-Å aluminum oxide films, our experiments and theoretical modeling confirm the presence of an additional mode at $\sim$800 cm^{-1} and the splitting of the 400-cm^{-1} feature into two peaks at about 350 and 500 cm^{-1} for our somewhat thicker 30-Å well-annealed α-Al_2O_3 films. The primary beam-energy dependence for the $\sim$900-cm^{-1} phonon is found experimentally to be $E^{-0.9}$ while the dielectric theory predicts $E^{-0.8}$, in contrast to the well known $E^{-0.5}$ dependence for bulk ionic crystals. The 800- and 900-cm^{-1} features are related to the high-frequency surface-phonon branches corresponding to the 650-cm^{-1} bulk TO modes and are expected from dielectric theory for an ideal alumina layer on metal support. The 350-, 500-, and 650-cm^{-1} modes are related to the low-frequency surface-phonon branches, which are allowed due to a $(\omega,\mathbf{k})$-dependent dispersion-related symmetry-mixing process. Successful modeling of these latter modes is carried out under the assumption of a "self-supported" alumina film.

I. INTRODUCTION

Aluminum oxide films are of broad importance in the fields of corrosion resistance and optics. The chemistry of the oxide surface is relevant to hydrocracking reactions and as a high surface area support for metals in catalysis. The vibrational and electronic properties of thin-film, as well as bulk, aluminum oxides have been extensively investigated.[1] However, the surface-phonon behavior, and hence the optical properties of thin alumina films, has not been understood in terms of the vibrational properties of the bulk oxide. For example, the surface phonons for oxygen in an Al(111) surface[2] measured with high-resolution electron-energy-loss spectroscopy (HREELS) exhibit three peaks at about 900, 650, and 400 cm^{-1}, whereas the surface phonons of single crystalline α-Al_2O_3(0001) (Ref. 3) show only two substantial features near 800 and 500 cm^{-1}.

Although a lightly oxidized Al(111) surface[2] yields a different crystal structure from α-Al_2O_3, the loss spectra are strikingly similar to Al_2O_3 thin films prepared by different methods.[4,5] The similarity between the phonon spectra of thin oxide films formed on either polycrystalline or single-crystal aluminum surfaces has been justified by Chen, Colaianni, and Yates[4] on the basis of an amorphous-to-crystalline oxide transition, which, to first order, is independent of the details of the structure of underlying Al at the interface. In recent work with ultrathin aluminum oxide films on Mo(110), Chen, Colaianni, and Yates[4] have questioned the assignment of the 400-cm^{-1} mode as an alumina phonon by demonstrating an enhancement of this feature with excess aluminum metal in the oxide film. We have subsequently shown that this phonon mode is not affected by complete oxidation (1 atm, 700 K) for a 30-Å film, but slowly decreases in intensity with extended annealing at higher temperatures (up to 1500 K in vacuum). It is concluded to be related to thin film or crystal defect structure rather than excess aluminum metal.[5] The decrease in the 400-cm^{-1} region does not correlate with the γ to α phase transition, either, as indicated by Auger parameter and valence-band measurements.[5] Chen, Colaianni, and Yates[4] assume a γ-Al_2O_3 structure, and call for calculation of the surface phonon modes of thin films based upon the γ-Al_2O_3 defect spinel structure. We have shown,[5] however, that the γ to α transition occurs at least as low as 1073 K for our 20–30-Å films, and may start as low as 900 K. No experimental evidence was available to determine crystal phase in the work of Chen, Colaianni, and Yates[4] but we suspect that their 1200-K, 1-h annealing procedure is probably quite sufficient to produce the α phase for their similarly thin films. The present experimental and theoretical work, based on optical constants from single-crystal α-Al_2O_3 (sapphire), should be relevant to the work of Chen, Colaianni, and Yates given both the similarity in phonon spectra and

thermal treatment of the films. The lower symmetry of the α-Al_2O_3 structure versus the $p(1\times1)$ O/Al(111) structure results in six phonon modes[3] rather than three,[2] with the two higher-frequency modes being somewhat anisotropic.[3] Although the thin-film and $p(1\times1)$-O structures cannot be compared rigorously, the similarity in the HREELS phonon spectra is remarkable. In fact, the phonon spectra of O/Al(111),[2] and various thin-film oxides such as amorphous γ-Al_2O_3, crystalline γ-Al_2O_3, and crystalline α-Al_2O_3, are to first order very similar[5] but differ considerably from the surface phonon spectrum of bulk α-Al_2O_3. To understand the various experimental observations, we must take into account the effects of film thickness, phonon dispersion, and substrate dielectric properties on the Fuchs-Kliewer modes. In this work, we show that the dependence of the long-wavelength surface phonons on these factors can be understood in the context of a macroscopic dielectric theory.

The early theoretical work of Fuchs and Kliewer[6] showed that the surface-phonon modes of a thin slab are directly tied to the bulk lattice behavior, and are a consequence of the boundary conditions at the surface. For the simple case of a single-oscillator isotropic lattice, there are two surface-phonon branches ω_+ and ω_-, which approach the bulk LO and TO frequencies, respectively, at Γ in the thin-film limit. With increasing film thickness and phonon wave vector the two branches converge at an intermediate frequency given by the Lyddane-Sachs-Teller relation. Good agreement is found with experiments on bulk ZnO and MgO single crystals.

For multiple-oscillator and anisotropic crystal structures, Lucas and Vigneron[7] have developed the so-called dielectric theory of electron-energy-loss spectroscopy (hereafter, simply the "dielectric theory") to calculate the surface-phonon structure, given the bulk dielectric tensor of the material. The agreement between theory and experiment is very good for a number of ionic single crystals, including α-Al_2O_3(0001), SiO_2(0001), MgO(001), NaCl(001), LiF(001), and UO_2(111).[8] The theory quantitatively predicts the surface-phonon frequencies and intensities. The dependence of the phonon loss intensity on the primary beam energy $\sim E_p^{-0.5}$ is also confirmed by experiments on single crystals of α-Al_2O_3 (Ref. 9) and ZnO (Ref. 10) and for 950-Å SiO_2/Si(100).[8] The primary beam-energy dependence has not been discussed as a function of film thickness, although adsorbed dipolar molecules display an E_p^{-1} dependence. We have recently reported a dependence of $\sim E_p^{-0.93}$ for the 900-cm^{-1} surface phonons of a 30-Å α-Al_2O_3 film on Ru(001),[5] and now will show that this behavior is predicted by an extension of the dielectric theory for thin films.

The extension of the theory to surface modes of thin films and multilayered materials has been developed by Lambin, Vigneron, and Lucas[11] and compared with GaAs/$Al_xGa_{1-x}As$ superlattices with layer thicknesses of 100 Å.[12] The multilayer model can be applied to the simple two-layer situation, where a film of thickness d_1 and dielectric function $\epsilon_1(\omega)$ is supported on a substrate of dielectric function $\epsilon_s(\omega)$. We are aware of several studies in which the spectra of thin films have been compared with theory. Onuki, Iwamoto, and Onaka[13] have compared the phonon spectra of LiF films evaporated on gold-coated glass substrates with the original slab calculations of Fuchs and Kliewer.[6] Although no attempt was made to account for the effects of the substrate, general agreement with the theory was obtained. However, it is interesting that the intense phonons observed are the lower-frequency modes which, for small phonon wave vectors, should not be dipole active on a metallic substrate. The gold thickness and the symmetry of the two surface-phonon branches were not discussed in their paper. Liehr *et al.*[14] have measured the thickness dependence of the surface-phonon frequency of an epitaxial CaF_2 film on Si(111). Although the phonon frequency in the thin-film regime (10–300 Å) is higher for thinner films, it is not in quantitative agreement with theory; they attribute the discrepancies to strain caused by a lattice mismatch between epitaxial CaF_2 and Si. A third example, thick amorphous SiO_2 layers thermally grown on Si(100),[15] shows more contradictory results. The phonon frequency dependence observed is a shift to lower frequency with decreasing film thickness below $\sim$55 Å. Theory predicts the opposite behavior.

In this paper, we present experimental phonon spectra of α-alumina films on a Ru(001) substrate. Aluminum metal was evaporated onto the clean Ru(001) crystal in UHV, then oxidized in air at 1 atm to form crystalline γ-Al_2O_3 films. Subsequent thermal annealing in UHV transformed the oxide to α phase. Auger parameter and valence-band measurements confirmed the phase characterization. Details of the thin-film phase and hydroxylation behavior were reported previously.[5] We compare the phonon spectra with the results of dielectric theory calculations of both polycrystalline and oriented crystalline films of aluminas "self-supported" and supported on a metal substrate. We found that the theory predicts a change in the phonon intensity dependence with primary beam energy from $E_p^{-0.5}$ for bulk to $E_p^{-0.80}$ for 10-Å films. This is in substantial agreement with the experimental determination of $\sim E_p^{-0.93}$, and represents a feature of the theory which has not been previously discussed or confirmed. The frequency shifts of the phonon modes of these Al_2O_3 films as a function of thickness were also in agreement with the dielectric theory unlike the initial oxidation of Si,[16] and the SiO_2/Si work discussed above.[15] However, modes in the 400- and 650-cm^{-1} regions were not expected to be surface dipole active for the ideal planar oxide-metal system based upon the dielectric theory. We discuss the excitation of both modes in terms of a dispersion related symmetry mixing process. This interpretation is supported by recent measurements of the relative phonon intensities with phonon wave vector by varying the primary beam energy.[17]

II. METHODS

A. Experiment

The preparation of the aluminum oxide films on the refractory Ru(001) substrate as well as the capabilities of

the Vacuum Generators ESCALAB/HREEL spectrometer used in this work have been described previously.[5] Briefly, Al was evaporated in UHV onto a precleaned and annealed Ru crystal. Subsequent oxidation could be performed with conditions from 1073-K and 10^{-6}-Torr O_2 in the preparation chamber to 700-K and several-Torr O_2-H_2O mixtures in the fast entry lock, or at 723-K and 1-atm air in an external oven. Annealing was performed in UHV to 1300 K, or in a separate high-vacuum oven to 1500 K. Film thicknesses were determined from x-ray photoelectron spectroscopy measurements of the Ru and Al core levels before and after oxidation of the Al films, yielding estimates consistent to within several percent. Oxide phase was indicated by comparison of the upper valence-band features and the Al Auger parameter with the bulk powder data of Kao and Merrill.[18] Elimination of residual metallic aluminum under extreme oxidation conditions was most sensitively determined by the Al(KLL) Auger line (1386 eV), which has a much larger inelastic mean free path ($\sim$25 Å) than the Al(LVV) line (68 eV, $\sim$7 Å).[19] The insensitivity of the surface-phonon structure to elimination of underlying metal has been thoroughly discussed elsewhere.[5] HREELS measurements were performed with a Vacuum Generators LEELS 400 unit. An incident beam angle of 45° relative to the surface normal was employed for most of the work, and elastic peak intensities of 10^4 counts/s with a resolution of $\sim$70–80 cm^{-1} were achieved for well-annealed 30-Å films. All experimental data were digitally acquired.

B. Dielectric theory

Calculations were performed based upon the theory of Lucas *et al.*[7] The single-phonon loss spectrum, referred to as the classical loss function P_{cl}, requires a double integration of the surface loss function $P(\omega,\mathbf{k},d_1)$ over all phonon wave vectors $\mathbf{k}$, which scatter the electron into the finite spectrometer half-acceptance angle ϕ_a, while conserving both energy and momentum:

$$P_{cl}(\omega)=\frac{8e^2}{\pi^2\hbar v_\perp}\int_0^{k_c}\int_0^{\Phi(k)}\frac{(kv_\perp)^3}{k^2[(\omega-kv_\parallel\cos\phi)^2+(kv_\perp)^2]^2}P(\omega,k,\phi,d_1)d\phi\,k\,dk\ , \tag{1}$$

where k and ϕ are the magnitude and polar angle of the phonon wave vector with respect to the forward-scattering direction; $v_\parallel$ and $v_\perp$ are the incident electron velocity components parallel and perpendicular to the surface; and the integration over ϕ is performed first analytically[11] if the surface loss function P is independent of ϕ. The loss function generates peaks at frequencies ω, when the effective dielectric function $\xi_0(\omega,k,d_1)=-1$:

$$P(\omega,k,\phi,d_1)=\mathrm{Im}\left[\frac{-1}{\xi_0(\omega,k,\phi,d_1)+1}\right]\ . \tag{2}$$

For the layer model,[11] ξ_0 is dependent upon the magnitude, but not necessarily on the polar angle ϕ of the excited phonon wave vector. For a circular analyzer entrance slit, the projection of allowed phonon wave vectors is an ellipse. To perform the ϕ integral first, the upper limit is given by

$$\Phi(k)=\begin{cases}\pi, & k\le k_c\cos\phi_i\\ \arcsin\left[\dfrac{\left[1-\left[\dfrac{k_c\cos\phi_i}{k}\right]^2\right]^{1/2}}{\sin\phi_i}\right], & k>k_c\cos\phi_i\ ,\end{cases} \tag{3}$$

where the cutoff wave vector in the scattering plane is given by $k_c=k_e\phi_a$, k_e is the incident electron wave vector, and the incident beam makes an angle ϕ_i with respect to the surface normal. Although our analyzer aperture is actually a rectangular slit, rather than the circular slits used in other spectrometers, the calculations were performed with an elliptical domain for several reasons. Comparison of phonon loss data, collected for Al_2O_3 films with various instruments, yields similar results indicating that aperture geometry does not strongly influence the observed spectrum. Examination of the integrand in Eq. (1) shows that energy and momentum conservation results primarily in forward scattering of the phonon, and that, with the beam energies and phonon frequencies involved, the cutoff in the k_x direction is more important than in the longer direction of our rectangular aperture k_y, i.e., perpendicular to the scattering plane. Furthermore, when the effective dielectric function is independent of ϕ in the k_x,k_y plane, the ϕ integration can be evaluated analytically as shown in Appendix 1 of Ref. 11, saving considerable computational time.[20]

The effective dielectric function $\xi_0(\omega,k,d_1)$ is given as[11]

$$\xi_0(\omega,k,d_1)=\epsilon_1(\omega)\frac{\epsilon_1(\omega)\tanh(kd_1)+\epsilon_s(\omega)}{\epsilon_s(\omega)\tanh(kd_1)+\epsilon_1(\omega)}\ , \tag{4}$$

where $\epsilon_1(\omega)$ is the first layer *isotropic* dielectric function, and $\epsilon_s(\omega)$ is the substrate (isotropic) dielectric function. Polycrystalline α-Al_2O_3 films were treated with an isotropic "average" dielectric function $\epsilon_{av}(\omega)$;

$$\epsilon_{av}(\omega)=\frac{2\epsilon_\perp(\omega)+\epsilon_\parallel(\omega)}{3}\ , \tag{5}$$

where the parallel and perpendicular components were

defined by sums over classical oscillator frequencies $\omega_{\mathrm{TO},i}$, oscillator strengths S_i, and damping constants γ_i:

$$\epsilon(\omega)=\epsilon_\infty+\sum_{i=1}^{n}\frac{S_i\omega_{\mathrm{TO},i}^2}{(\omega_{\mathrm{TO},i}^2-\omega^2-i\omega\gamma_i)} . \tag{6}$$

A Drude model was used to describe the metal substrate,

$$\epsilon_s(\omega)=1.03-\frac{\omega_p^2}{\omega^2+i\omega/\tau} \tag{7}$$

using the values $\omega_p=14.7$ eV and $\tau=0.801\times10^{-14}$ s for aluminum.[21] Variation of the plasma frequency from Al-like ($\sim$15 eV) to Ru-like ($\sim$30 eV) showed no changes in the surface-phonon structure. Interface phonons are not expected since the dielectric functions of the film and the substrate are so different. For self-supported films, the substrate dielectric function is simply set equal to $\epsilon_{\mathrm{vac}}=1$. Note that, in the limit of infinite film thickness, the effective dielectric function $\xi_0(\omega)$ in Eq. (4) reduces to $\epsilon_1(\omega)$.

To treat oriented films of the anisotropic oxide, the dielectric tensor is written in the following block form:[22]

$$\boldsymbol{\epsilon}_1(\omega,\mathbf{k})=\begin{bmatrix}\boldsymbol{\epsilon}_{\rho\rho} & \boldsymbol{\epsilon}_{\rho z}\\ \boldsymbol{\epsilon}_{z\rho} & \epsilon_{zz}\end{bmatrix} , \tag{8}$$

where

$$\boldsymbol{\epsilon}_{\rho\rho}=\begin{bmatrix}\epsilon_{xx} & \epsilon_{xy}\\ \epsilon_{yx} & \epsilon_{yy}\end{bmatrix},\quad \boldsymbol{\epsilon}_{\rho z}=\begin{bmatrix}\epsilon_{xz}\\ \epsilon_{yz}\end{bmatrix} . \tag{9}$$

The effective dielectric function $\xi_0(\omega,k,d_1)$ is then given as

$$\xi_0(\omega,k,d_1)=a-\frac{b^2}{c+\epsilon_s} , \tag{10}$$

where

$$a=\epsilon_{zz}\frac{\alpha}{k}\coth(\alpha d)+i\boldsymbol{\epsilon}_{\rho z}\cdot\mathbf{k}/k , \tag{11}$$

$$b=\frac{\epsilon_{zz}\alpha}{k\sinh(\alpha d)} , \tag{12}$$

$$c=\epsilon_{zz}\frac{\alpha}{k}\coth(\alpha d)-i\boldsymbol{\epsilon}_{\rho z}\cdot\mathbf{k}/k , \tag{13}$$

$$\alpha=\frac{-i\mathbf{k}\cdot\boldsymbol{\epsilon}_{\rho z}+[\epsilon_{zz}(\mathbf{k}\cdot\boldsymbol{\epsilon}_{\rho\rho}\cdot\mathbf{k})-(\mathbf{k}\cdot\boldsymbol{\epsilon}_{\rho z})^2]^{1/2}}{\epsilon_{zz}} . \tag{14}$$

The uniaxial tensor for α-Al_2O_3, with the c axis making an angle θ with respect to the z axis, is written

$$\boldsymbol{\epsilon}=\begin{bmatrix}\epsilon_\parallel\sin^2\theta+\epsilon_\perp\cos^2\theta & 0 & (\epsilon_\parallel-\epsilon_\perp)\sin\theta\cos\theta\\ 0 & \epsilon_\perp & 0\\ (\epsilon_\parallel-\epsilon_\perp)\sin\theta\cos\theta & 0 & \epsilon_\parallel\cos^2\theta+\epsilon_\perp\sin^2\theta\end{bmatrix} . \tag{15}$$

For the case of $\hat{\mathbf{c}}$ normal to the surface, the ϵ_{zz} component is simply $\epsilon_\parallel$, $\boldsymbol{\epsilon}_{\rho z}$ is zero, and ξ_0 is independent of ϕ, so that the ϕ integration can be performed analytically as noted above. The theoretical spectra shown in this paper were calculated with the optical constants of Liehr *et al.*,[3] compiled in Table I. Spectra calculated with the IR constants of Barker[23] were not substantially different.

TABLE I. Values of the IR constants describing the dielectric function $\xi_0(\omega)$ in Eq. (2), for α-Al_2O_3.

Mode	$\omega_{\mathrm{TO},i}$	S_i	γ_i	ω_{LO}
$\epsilon_\parallel$:		$\epsilon_\parallel(\infty)=3.2$		
1	390	6.5	14	512
2	578	1.9	55	871
$\epsilon_\perp$:		$\epsilon_\perp(\infty)=3.08$		
3	381	0.3	6.0	388
4	438	2.8	4.0	480
5	568.5	3.0	30.0	625
6	639.5	0.3	39.0	900

Given that the dielectric theory is a macroscopic theory, several questions regarding the range of applicability should be addressed. First, energy and momentum conservation requirements show that for a high-frequency mode $\omega=900$ cm^{-1} and a beam energy of several eV, the associated phonon wave vector will be on the order of 0.002 Å^{-1}, corresponding to a wavelength of 500 Å. As a consequence of the long wavelengths resonantly excited, a classical description is warranted. The decay of these surface modes into both the bulk and vacuum is also characterized by a length comparable to the wavelength and indicates why the surface loss function can be sensitive to dielectric properties as deep as 10^3 or 10^4 Å. The question of validity of the dielectric theory in the thin-film limit has been addressed by comparison with lattice-dynamics calculations for the NaF case. Frequency shifts were in agreement down to about 20 Å, and relative intensities to even lower thickness.[24] Mixing of the classical Fuchs-Kliewer modes with bulk LO subbands produced multiplet splittings, which would not be at present experimentally observable but could contribute to the broadening of thin-film loss features. General agreement between the frequencies predicted and observed for our Al_2O_3 films in the 20–30-Å regime will serve to justify this work. Of more serious concern is the limitation on magnitude of the phonon wave vector. Comparison of lattice-dynamics calculations with the dielectric theory showed for NaF slabs on a Si substrate that for films as thin as 8 Å agreement was found below 0.005 Å^{-1}.[24] The validity at larger wave vectors is limited by dispersion and symmetry mixing as will be shown below.

III. EXPERIMENTAL RESULTS

We show in Fig. 1 the surface phonon spectra for several phases of aluminum oxide supported on the Ru(001) substrate. Spectrum *A* is a 20-Å film oxidized in a H_2O-O_2 mixture at 298 K, resulting in an amorphous γ-like alumina. Curve *B* is the spectrum for a 35-Å crystalline γ oxide film, prepared at 700 K in air, then cleaned in O_2 and dehydroxylated at 773 K in the UHV system. The γ phase characterization has been discussed previously,[5] and was based upon the Al Auger parameter (1461.6 eV) and upper valence-band features which compared very well with dispersed alumina powders of known phase.[5,18] Curve *C* shows the phonon spectrum of

a film annealed to 1073 K, resulting in an α-phase Auger parameter (1461.9 eV) but retaining considerable intensity in the 400-cm^{-1} region. Curve *D* shows the sample after extensive annealing at temperatures up to 1523 K, resulting in well-annealed α-Al_2O_3. The phase transition was again characterized by the Auger parameter (1461.9 eV) and valence-band features. The transition to α-phase occurred by 1073 K, several hundred degrees lower than the bulk transformation temperature.[25] The lower γ to α phase transition temperature for thin films[26] and small particles[27] has been observed by others, and probably is related to defect-enhanced kinetics in the nucleation and growth mechanism. We point out that the three major features in the single phonon spectra, at 400, 650, and 900 cm^{-1}, do not change dramatically with thermal treatment between the amorphous-γ and the final α-Al_2O_3 phase. With extended annealing, the 400-cm^{-1} mode clearly decreases in intensity relative to the other two, and a shoulder near 800 cm^{-1} develops on the low-frequency side of the 900-cm^{-1} peak. As discussed above, metallic aluminum in the oxide lattice can enhance the 400-cm^{-1} intensity.[4] However, we have monitored residual Al^0 spectroscopically following vigorous oxidation treatments (1 atm, 700 K, $\frac{1}{2}$ h) (Ref. 5) and have demonstrated that the elimination of underlying Al^0 does not decrease this mode, but rather its intensity is related to extended annealing of the oxide film at temperatures between 1100 and 1300 K.

The dependence of the ~900-cm^{-1} phonon peak intensity on primary beam energy is related to the scattering mechanism involved as well as the dielectric properties of the sample. In contrast to the $E_p^{-0.5}$ dependence for surface phonons of bulk ionic single crystals, we show in the inset of Fig. 1 an approximately $E_p^{-0.93}$ dependence measured for a well-annealed 30-Å α-Al_2O_3 film/Ru(001). Also shown are dashed lines for the limiting cases expected for surface phonons of bulk crystals ($E_p^{-0.5}$) and for a layer of adsorbed dipoles ($E_p^{-1.0}$).

We have noted a systematic decrease in the 400- and 650-cm^{-1} phonon intensities relative to the 900-cm^{-1} mode as the primary beam energy is increased.[17] Energy and momentum conservation considerations imply that the magnitude of the sampled phonon wave vector is proportional to $E_p^{-1/2}$, showing that this is a dispersion-related effect. As we change the primary beam energy from 3 to 30 eV, the relative intensity of the 650- to 900-cm^{-1} mode drops by a factor of ~$\frac{1}{3}$. The 900-cm^{-1} mode also shifts to slightly higher frequency with increasing beam energy.

More subtle changes in the phonon structure, observed over the course of various sample treatments and instrumental tune-ups, are summarized in Fig. 2. Deconvolution of the measured elastic peak line shape from each phonon loss spectrum (solid curve) results in the dashed curves, which more clearly delineate the spectral features.

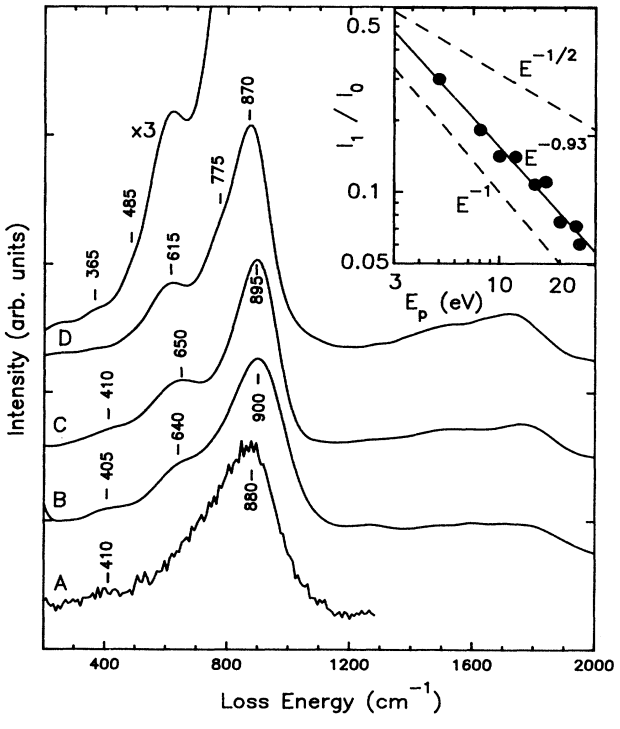

FIG. 1. HREELS phonon spectra of different phases of oxide on Ru(001). *A*, amorphous γ-like; *B*, crystalline γ; *C*, 1073-K annealed α-Al_2O_3; and *D*, 1523-K annealed α-Al_2O_3. The inset shows the dependence of the one-phonon–to–elastic-peak-intensity ratio on primary beam energy E_p for the high-frequency (~880-cm^{-1}) mode for a 30-Å α-Al_2O_3 film. Dashed lines correspond to E^{-1} (adsorbed dipole layer) and $E^{-1/2}$ (bulk crystal surface phonon) behavior.

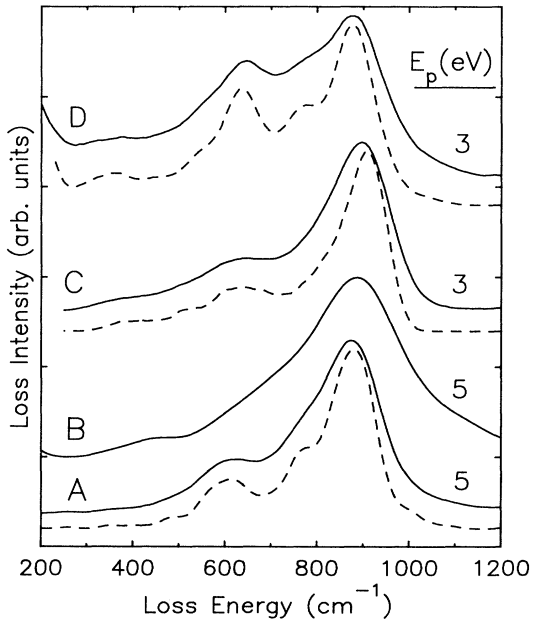

FIG. 2. HREELS phonon spectra of α-Al_2O_3 films: *A*, 1523-K annealed, $E_p = 5.0$ eV spectrum; *B*, sputtered with Ar^+ (1 kV, 20 μA, 2 min); *C*, typical annealed, $E_p = 3.0$ eV spectrum; and *D*, spectrum showing enhancement of ~800-cm^{-1} feature. The solid curves are original digitally acquired data. The dashed curves are the result of resolution enhancement.

The resolution enhancement analysis was based upon the nonlinear predictor method of maximum likelihood.[28] Because the actual spectrometer line shape is experimentally determined for each loss spectrum, there is a high level of confidence for the deconvolution as has been shown in other HREELS studies.[29] As has been seen before,[2] light sputtering of the surface leads to a preferential decrease in the 650-cm^{-1} mode [Fig. 2(b)] relative to the well-annealed surface [Fig. 2(a)]. The small shoulder observed on the low-frequency side of the 900-cm^{-1} phonon [Fig. 2(c)] increased significantly, as shown in Fig. 2(d) after sputtering and annealing. The feature at about 400 cm^{-1} has also been observed to split into two subbands at ~350 and 500 cm^{-1} [Figs. 2(a), 2(c), and 2(d)]. The observation of these phonon features will be discussed in light of the calculational results below. We note that a shoulder near 800 cm^{-1} and a small but observable 400-cm^{-1} mode are also detectable in data from ultrathin alumina on molybdenum.[4]

IV. THEORETICAL RESULTS

The oxide thickness dependence of the surface-phonon frequencies and intensities are shown in Figs. 3 and 4, for the oxide on an aluminum metal substrate and self-supported, respectively. Several features of the thickness dependence are understandable from Fuchs and Kliewer's original work with the simpler single-oscillator, isotropic, NaCl lattice-type slab model. For each fundamental optical vibration of the ionic crystal, there are two TO modes and one LO mode. The surface phonon in an "infinitely" thick sample lies somewhere between the bulk LO and TO frequencies. As the sample gets thinner,

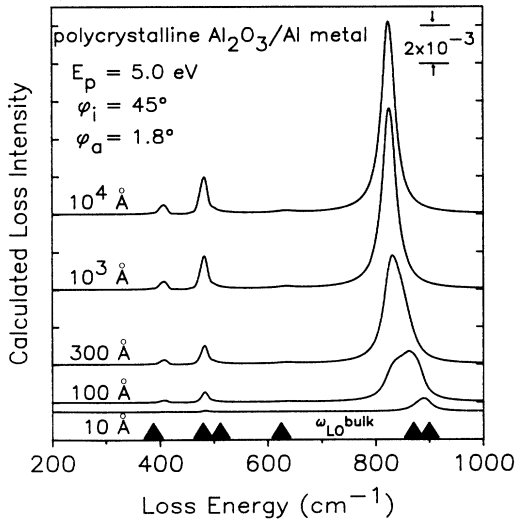

FIG. 3. Calculation of the classical loss function for vacuum–oxide–Al-metal model systems with the indicated oxide thicknesses. The "average" polycrystalline dielectric function for the oxide is indicated in Eq. (5). The vertical scale divisions represent 2×10^{-3} cm. The triangles at the bottom indicate the (zero damping) frequencies of the bulk LO modes.

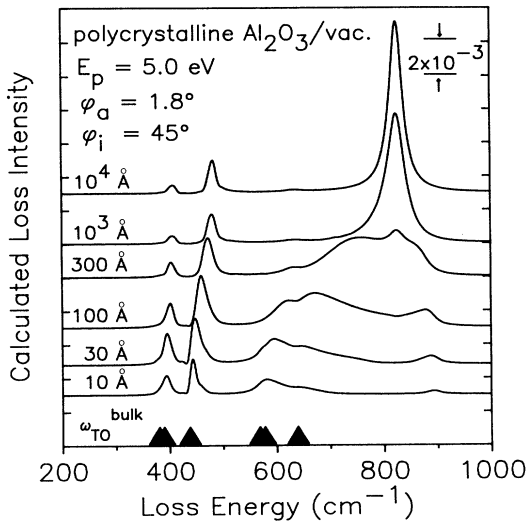

FIG. 4. Calculation of vacuum-oxide-vacuum model systems with the indicated oxide film thicknesses. The average polycrystalline dielectric function for the oxide is indicated in Eq. (5). Spectra are shifted vertically for clarity; 1 division represents 2×10^{-3} cm. The triangles at the bottom indicate the (zero damping) frequencies of the bulk TO modes.

the surface mode splits its degeneracy and the higher-frequency branch (ω_+) moves up to the bulk LO frequency, while the lower-frequency branch (ω_-) shifts down to the bulk TO frequency at zero thickness. Focusing on the highest frequency bulk modes (2 and 6, Table I), which have large oscillator strengths and thus large frequency shifts between the LO and TO bands, the corresponding surface phonons in Fig. 3 shift to higher frequency and decrease in intensity with decreasing oxide slab thickness. As expected in the thin-film limit, the high-frequency branch approaches the bulk LO frequency. Although the other surface modes in Fig. 3 do not shift as dramatically, their positions are approximately at the bulk LO frequencies as indicated by the triangles.

At the Γ point, the surface phonons can be strictly divided into LO and TO symmetries.[6] The motion of the high-frequency surface phonon is actually transverse in nature, while the low-frequency surface phonon is longitudinal in motion, opposite in symmetry to the bulk modes.[6] When sampling wave vectors away from Γ, the symmetries mix and each branch can be resolved into three components (one longitudinal and two transverse), of which only the transverse motion normal to the surface is dipole active on a metallic substrate. The longitudinal motion and the transverse motion parallel to the surface are canceled by the presence of the image dipole in the metal support when averaged over the surface. Therefore, for oxide on metal, only the high-frequency branches are expected at or near Γ in the thin-film limit from the classical dielectric theory.

Removal of the metal substrate from the oxide film allows the low-frequency branches to contribute within the dielectric theory. The classical loss function for 10- and 30-Å films plotted in Fig. 4 is dominated by the more in-

tense low-frequency modes, whose positions approach the bulk TO modes as indicated. Although the high-frequency branches are still allowed, only the strongest mode at ~ 890 cm^{-1} can be seen, due to the greater intensity of the low-frequency branches. Whereas the high-frequency branches shift to lower frequency with increasing film thickness, the low-frequency branches all shift to higher frequency in agreement with the general behavior given by Fuchs and Kliewer. The 10^4-Å film is again bulklike, and as expected, coincides with the spectrum shown for a 10^4-Å film in Fig. 3.

It is clear at this point that, although the dielectric theory has given quantitative agreement with surface phonons of bulk ionic crystals, the correspondence between the measured phonon spectra of Figs. 1 and 2, and the calculations of Fig. 3 for oxide-on-metal is convincing only for the two phonons between 800 and 900 cm^{-1}. Intensity observed in the 400- and 650-cm^{-1} regions cannot be accounted for with oxide-metal calculations using various primary beam energies, film thicknesses, incident beam angles, spectrometer slit sizes, polycrystalline effects, or crystalline film orientations. However, reasonable phonon positions and intensities are accounted for in these regions if we calculate the phonon spectrum for the self-supported oxide film as shown in Fig. 4. To illustrate the effect of different orientations of a single-crystal film on the phonon modes, calculations were performed for the optical c axis parallel and perpendicular to the surface, as indicated in Fig. 5, using the dielectric theory cast in a tensor form as indicated in Eqs. (8)–(15). The

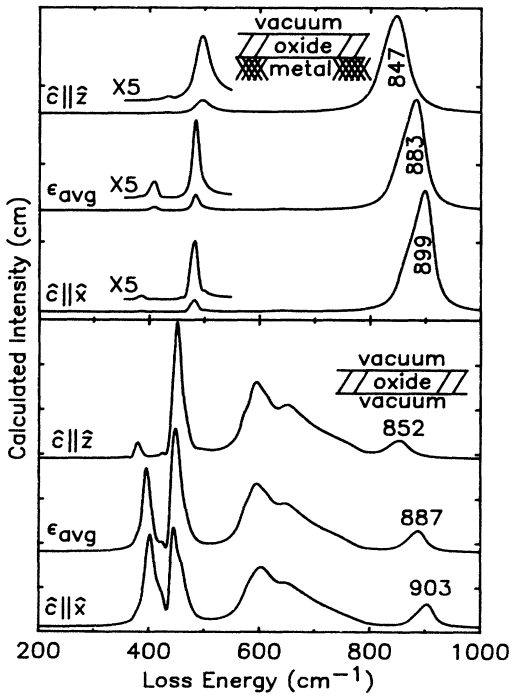

FIG. 5. Upper section compares $\hat{c}\|\hat{x}$, $\hat{c}\|\hat{z}$, and polycrystalline alumina films on a metallic Al substrate; the lower section compares "self-supported" films for the same orientations.

upper section of Fig. 5 compares two oriented 30-Å films of oxide on an aluminum substrate with a 30-Å polycrystalline film on aluminum. The substantial shift between 899 cm^{-1} ($\hat{c}$ in the plane of surface) and 847 cm^{-1} ($\hat{c}$ normal to the surface) of the strongest phonon mode is simply a consequence of the anisotropy of the α-Al_2O_3 crystal. While the lower-frequency modes also shift with orientation, dramatic intensity increases in the 400- and 650-cm^{-1} regions are not observed. The lower section of Fig. 5 compares calculations of two oriented 30-Å self-supported oxide films with the self-supported polycrystalline 30-Å film. The notable difference between the $\hat{c}$-normal and $\hat{c}\|\hat{x}$ spectra is the relative intensities of the two lowest-frequency surface phonons. Although the splitting between these peaks is comparable to the achievable resolution on these thin films, the theory predicts an observable difference between the two orientations, or between the $\hat{c}$-normal [α-$Al_2O_3(0001)$] and a polycrystalline surface.

We now turn to the dependence of phonon intensity on the primary beam energy E_p and its relationship to film thickness. The primary beam energy dependence predicted and observed for surface phonons of bulk crystals is $E_p^{-0.5}$. The general understanding seems to be that this is a *long-wavelength phonon* characteristic where the excitation is primarily the long-range dipole scattering mechanism.[30] For reference, the dipole scattering of a layer of adsorbed dipolar molecules shows an E_p^{-1} behavior, and was modeled within the dielectric theory as a layer with dielectric constant ϵ_d on a metal substrate.[10] In contrast, the impact scattering mechanism has an E_p^{+1} dependence.[10] An experimental energy dependence for ionic thin films (less than ~ 1000 Å) had not been reported previously.

Our experimental result[5] for a 30-Å film on Ru(001) of $\sim E_p^{-0.93}$ was therefore surprising. However, given that the dependence for adsorbed dipolar molecules was derived by assuming a dielectric layer on a metal substrate, we applied the dielectric theory two-layer model to this question of energy dependence. Figure 6 shows the calculations of the 800–900-cm^{-1} region using primary beam energies of 5, 10, 20, and 40 eV for a range of film thicknesses. The presence of two distinct surface phonons near the frequencies of the two bulk LO modes indicated in Fig. 3 can now be seen for different film thicknesses and beam energies. The higher-frequency mode is favored for the thinner film thicknesses and higher beam energies. In Fig. 7 we plot the intensities of these phonon peaks after convolution with a Gaussian (full width at half maximum of 64 cm^{-1}) representing our instrumental resolution versus beam energy for each thickness to obtain the observable energy dependence. At low beam energies, the broadening of the dipolar lobe results in a decrease in the inelastically scattered electrons collected by the finite aperture of the analyzer which accounts for the slight nonlinearity.[10] Nevertheless, linear fits give an approximate description of the energy behavior and are sufficient within the accuracy of experimental measurement. The slopes of the log-log plot are summarized in Fig. 8 along with the frequency and intensity variation of the convoluted spectra over the

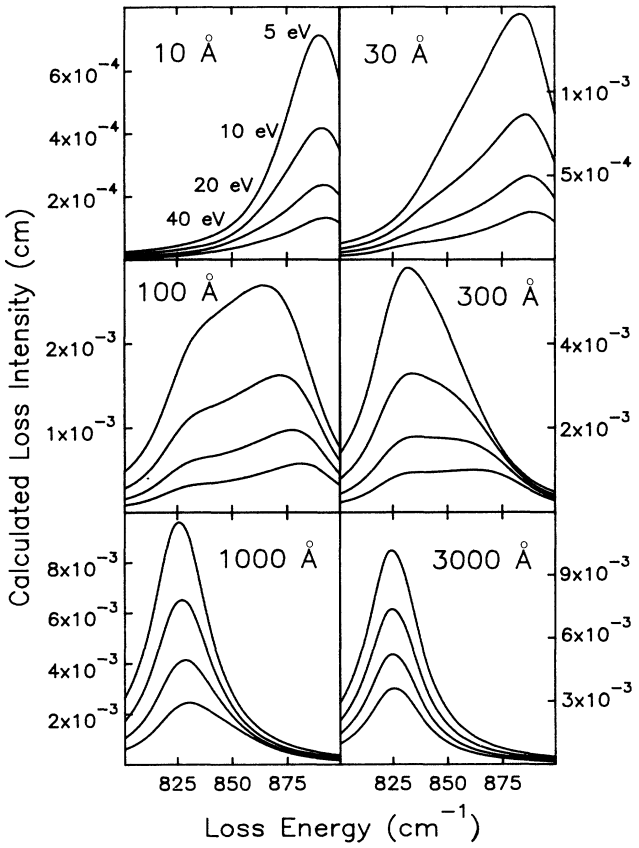

FIG. 6. Primary beam-energy dependence of the highest-frequency phonon peak structure for films of the indicated thickness on a metallic Al substrate. Beam energies shown are 5, 10, 20, and 40 eV.

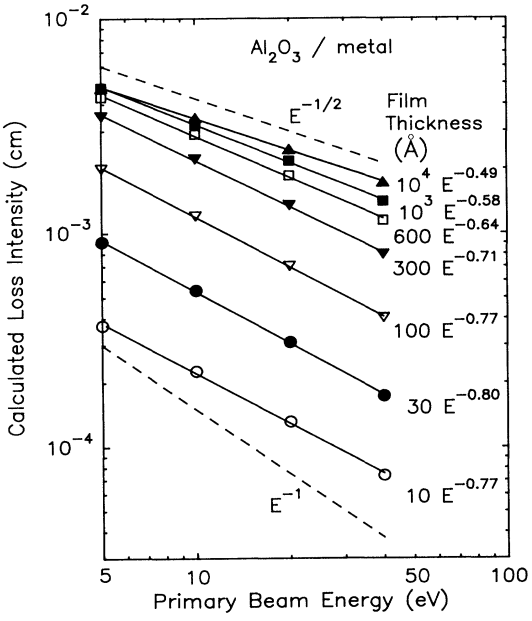

FIG. 7. Log-log plot of peak intensities vs primary beam energy for the phonon spectra shown in Fig. 6 after convolution with an instrumental resolution of 64 cm^{-1}.

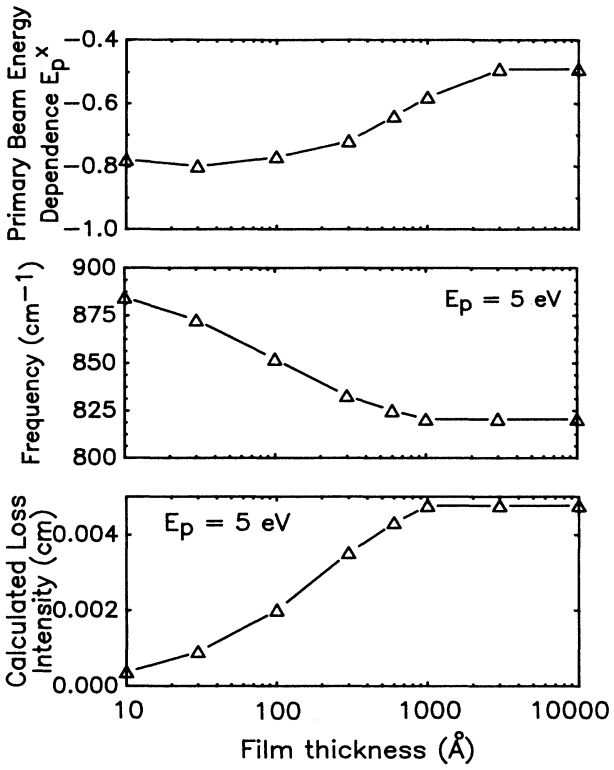

FIG. 8. Summary of the intensity, frequency, and beam-energy dependence on film thickness for the spectra of Fig. 6 after convolution with an instrumental resolution of 64 cm^{-1}.

thickness range. Examination of the energy dependence of the two modes, for example the 300-Å spectra in Fig. 6, shows that they do not decrease in intensity with increasing primary beam energy at the same rate. Thus, for higher instrumental resolution, a nonmonotonically increasing E_p behavior is predicted in the 100–300-Å range. Both ends of the thickness range are in good agreement with experiment, representing a feature of the dielectric theory which, to our knowledge, had not been previously proposed or established.

V. DISCUSSION

Because the alumina phase diagram is quite complex with subtle changes in the pseudocubic oxygen anion lattice, we felt that a thorough investigation of the surface phonons for a thin film of constant thickness but different phases was required. In fact, only relative intensity changes are observed, in contrast to calculations[5] of thin films using the IR constants of Chu *et al.*[31] which predict two modes for amorphous and four modes for γ alumina. Comparison of the effect of ion bombardment on the 650-cm^{-1} mode and the decrease in intensity of this mode in the amorphous film spectrum suggests that this mode is more sensitive to surface order than the other two modes. After annealing the sample, the more crystalline γ-like oxide shows quite definite features at about 390 and 650 cm^{-1}. Further annealing of the film

shows a slow decrease in the intensity of the low-frequency region, unlike the more abrupt change in the Auger parameter which marks the phase transformation. The steady decrease in intensity of the 400-cm^{-1} region might suggest that these modes should not be dipole active for the ideal α-Al_2O_3 film but are allowed by symmetry breaking processes in these real films. The 650-cm^{-1} feature persists with extended annealing (up to 5 h at 1523 K), and does not show a similar decrease in intensity. This presents a greater challenge to the predictions of the dielectric theory.

As can be seen from the dielectric theory calculations of Figs. 3 and 4, and as indicated by Fuchs and Kliewer, only the higher-frequency branch is expected for a thin film supported on a conductive substrate. Nevertheless, our own results as well as those of Onuki, Iwamoto, and Onaka[13] for 130–310-Å LiF films display peaks quite characteristic of the lower-frequency branches. Onuki, Iwamoto, and Onaka[13] have calculated the **k**-space dispersion relation, using Fuchs and Kliewer's results for films of varying thicknesses, and the wave-velocity matching condition for the electron. Because the reduced surface-phonon wave vector $\mathbf{S}=\mathbf{kd}$ is dependent on film thickness, for the case of their several-hundred-angstrom films, the wave-velocity matching condition is satisfied at a point which is not very close to $S=0$. Therefore the symmetries of the phonons at the wave-velocity matching point in the two branches are quite mixed, and both branches are dipole allowed. With the higher intensity predicted for the lower-frequency branch relative to the higher-frequency branch as well as their limited experimental resolution, only the lower frequency branch is resolved.

Our observation of a decrease in the 400- and 650-cm^{-1} regions relative to the 900-cm^{-1} mode with an increasing beam energy is a clear indication that dispersion accounts for the symmetry mixing.[17] The shift of the high-frequency 900-cm^{-1} branch to slightly higher frequency with increasing beam energy is also in agreement with this interpretation. The 650- and 900-cm^{-1} modes are identified as the low- and high-frequency branches, respectively, of modes 2 and 6 in Table I. The 400-cm^{-1} region probably consists of a mixture of the low-frequency branches of modes 1, 3, and 4 which are of smaller oscillator strength and have smaller LO-TO splittings than modes 2 and 6. The phase-matching condition will be satisfied further out in the surface-phonon dispersion curve for the 650-cm^{-1} mode than for the 400-cm^{-1} mode, which accounts for the greater contribution of the 650-cm^{-1} mode in comparison with the modes in the 400-cm^{-1} region.

This mixing of symmetries has also been predicted recently by Senet *et al.*[24] for NaF self-supported films. In a comparison of the macroscopic treatment of the oxide lattice modes in the dielectric theory with a microscopic approach, a mixing between the "classic" Fuchs-Kliewer surface modes and bulk LO subbands is observed for both the high- and low-frequency branches. A microscopic multiplet fine structure develops due to this mixing, which is beyond present experimental capabilities but supports our interpretation of a thin-film related symmetry mixing of our 400- and 650-cm^{-1} modes. Senet *et al.*[24] remark that the validity of the dielectric theory is limited to very small k vectors (~ 0.005 $Å^{-1}$), where this mixing of symmetries would be minimal. Our experimental sampling of k vectors falls well below this limit. Information about the surface-phonon modes can also be obtained from infrared reflection-absorption spectroscopy (IRAS). With p-polarized light, only the strong modes near 900 cm^{-1} are observed in alumina thin films.[32] In contrast, transmission spectra for the same films show absorption by the modes in the 650- and 400-cm^{-1} regions. The IRAS data support our analysis of the symmetry of these modes in the $k \rightarrow 0$ limit. Thus observation of modes in both the 650- and 400-cm^{-1} regions of HREELS spectra requires symmetry mixing due to dispersion effects.

The second aspect of the work which finds good agreement with the dielectric theory is the dependence of phonon intensity on primary beam energy. It is now clear that the $E_p^{-0.5}$ dependence is not a general surface phonon behavior, but is limited to thick, bulklike films and single crystals, where the first layer dielectric material thickness is larger than the wavelength of the phonon modes (typically 1 μm). That the dependence may vary with the frequency and strength of the oscillator mode is indicated in Fig. 6. The thin-film limit for the higher-frequency (890-cm^{-1}) mode of about $E^{-0.8}$ seems to be different from that of the lower-frequency (824-cm^{-1}) mode, and may be due to frequency—as well as symmetry—differences. The behavior of the self-supported Al_2O_3 films as well as self-supported MgO films also show differences between the low- and high-frequency branches.[33] However, because it is not clear how to treat the symmetry breaking observed experimentally within the dielectric theory, the energy dependence predicted for the lower-frequency branches remains somewhat unsubstantiated until beam-energy dependence measurements on films of intermediate thicknesses can be completed. For the higher-frequency branches, substantial agreement between experiment and theory has been found. We believe that this represents an aspect of the dielectric theory which had not been previously discussed. Detailed calculations based on this theory are in good agreement with our experimental results.

Previous experimental characterization of the phonon modes in thin ($\sim$10-Å) Al_2O_3 films[2,34] have only focused on the three most intense features. With somewhat thicker oxide films and extended annealing, we have repeatedly observed a shoulder at about 800 cm^{-1} and a splitting in the 350–500-cm^{-1} region which can be seen also in the data of Chen, Colaianni, and Yates.[4] We believe that the phonon spectrum of a well-annealed α-Al_2O_3 film can be distinguished from γ-Al_2O_3 and less-ordered α-Al_2O_3 films by these subtle changes which are a consequence of the slight anisotropy of the α-Al_2O_3 crystal structure. These features are well substantiated from the standpoint of the dielectric theory calculations given in Figs. 5 and 6, respectively. Furthermore, it is significant that the surface-phonon features can be related directly to the bulk phonons determined for the single crystal α-Al_2O_3.

VI. SUMMARY

HREELS investigations of well-characterized, single phase α-Al_2O_3 thin films have resolved several new phonon features not previously observed. Calculations based upon the "dielectric theory of electron-energy-loss spectroscopy" support the observed spectra and substantiate the variation with thickness of the primary beam-energy dependence of the phonon losses. The conclusions reached in this work are as follows.

(i) The main features in the surface-phonon spectrum are very similar for various phases of alumina.

(ii) The characteristic three-peak phonon spectrum commonly observed for thin film alumina has been verified to be due to oxide lattice vibrations, not to polycrystallinity effects, different oxide phases, or residual aluminum metal in thin films (20–100 Å). We do note that loss of intensity in the 400-cm^{-1} mode, which occurs with high-temperature annealing, may in part be due to a splitting of intensity into two features near 350 and 500 cm^{-1}. A shoulder near 800 cm^{-1} also appears with annealing. The features can be accounted for in the dielectric theory calculations and are truly characteristic of a "well-annealed" α-Al_2O_3 structure.

(iii) Calculations of the surface-phonon loss structure are substantially in agreement with experiment. The calculated primary beam-energy dependence for the ~900-cm^{-1} phonon mode of a 30-Å Al_2O_3 film ($E_p^{-0.8}$) is in good agreement with experiment ($E_p^{-0.9}$). The calculations of primary beam-energy dependence as a function of film thickness show that the often quoted $E_p^{-0.5}$ dependence is not a general surface-phonon behavior, but applies only to infinitely thick samples (≥ 1 μm).

(iv) The observation in HREELS of the two dominant modes at lower frequencies, i.e., 400 and 650 cm^{-1}, is primarily due to symmetry mixing with dispersion of the phonon modes away from the Γ point. Annealing of surface defects decreases the ~400-cm^{-1} mode intensity, indicating that defects may also contribute to symmetry mixing.

The application of the dielectric theory of EELS to these aluminum oxide films has provided a framework for understanding the surface phonons of thin film and bulk Al_2O_3 measured with HREELS and IRAS, despite limitations in its treatment of symmetry mixing. To date, this macroscopic model provides the most complete understanding of the thickness and energy dependence of thin-film oxide surface phonons.

ACKNOWLEDGMENTS

We gratefully acknowledge support from the National Science Foundation, Grant No. DMR 87-05680, and the Eastman Kodak Company.

*Author to whom correspondence should be addressed.

[1]I. P. Batra and L. Kleinman, J. Electron Spectrosc. Relat. Phenom. **33**, 175 (1984); D. L. Cocke, E. D. Johnson, and R. P. Merrill, Catal. Rev. Sci. Eng. **26**, 163 (1984).

[2]J. L. Erskine and R. L. Strong, Phys. Rev. B **25**, 5547 (1982); R. L. Strong, B. Firey, F. W. de Wette, and J. L. Erskine, *ibid.* **26**, 3483 (1982).

[3]M. Liehr, P. A. Thiry, J. J. Pireaux, and R. Caudano, J. Vac. Sci. Technol. A **2**, 1079 (1984).

[4]P. J. Chen, M. L. Colaianni, and J. T.Yates, Jr., Phys. Rev. B **41**, 8025 (1990).

[5]B. G. Frederick, G. Apai, and T. N. Rhodin, Surf. Sci. **244**, 67 (1991).

[6]R. Fuchs and K. L. Kliewer, Phys. Rev. **140**, A2076 (1965).

[7]A. A. Lucas and J. P. Vigneron, Solid State Commun. **49**, 327 (1984); A. A. Lucas, J. P. Vigneron, Ph. Lambin, P. A. Thiry, M. Liehr, J. J. Pireaux, and R. Caudano, Int. J. Quantum Chem. Quantum Chem. Symp. **19**, 687 (1986).

[8]P. A. Thiry, M. Liehr, J. J. Pireaux, and R. Caudano, J. Electron Spectrosc. Relat. Phenom. **39**, 69 (1986).

[9]J. J. Pireaux, P. A. Thiry, R. Caudano, and P. Pfluger, J. Chem. Phys. **84**, 6452 (1986).

[10]H. Ibach and D. L. Mills, *Electron Energy Loss Spectroscopy and Surface Vibrations* (Academic, New York, 1982), pp. 63–126 and 257–274.

[11]Ph. Lambin, J. P. Vigneron, and A. A. Lucas, Phys. Rev. B **32**, 8203 (1985).

[12]Ph. Lambin, J. P. Vigneron, A. A. Lucas, P. A. Thiry, M. Liehr, J. J. Pireaux, R. Caudano, and T. J. Kuech, Phys. Rev. Lett. **56**, 1842 (1986).

[13]H. Onuki, H. Iwamoto, and R. Onaka, Solid State Commun. **34**, 941 (1980).

[14]M. Liehr, P. A. Thiry, J. J. Pireaux, and R. Caudano, Phys. Rev. B **34**, 7471 (1986); P. A. Thiry, M. Liehr, J. J. Pireaux, R. Caudano, Surf. Sci. **189/190**, 373 (1987).

[15]P. A. Thiry, M. Liehr, J. J. Pireaux, R. Sporken, R. Caudano, J. P. Vigneron, and A. A. Lucas, J. Vac. Sci. Technol. B **3**, 1118 (1985).

[16]H. Ibach, H. D. Bruchmann, and H. Wagner, Appl. Phys. A **29**, 113 (1982).

[17]G. Apai, B. G. Frederick, and T. N. Rhodin (unpublished).

[18]C. C. Kao, Ph.D. thesis, Cornell University, 1988; R. P. Merrill (private communication).

[19]M. P. Seah and W. A. Dench, Surf. Interface Anal. **1**, 2 (1979).

[20]The calculations were performed using MathCAD 2.5 running on a PC-AT with an 80287 math coprocessor. Selected data points were also checked with SciMath and Derive on a Quadram 386XT accelerated PC-XT and with Mathematica on a Macintosh II.

[21]D. Y. Smith, E. Shiles, and M. Inokuti, in *Handbook of Optical Constants of Solids,* edited by E. D. Palik (Academic, Orlando, 1985), p. 395.

[22]A. A. Lucas, J. P. Vigneron, P. Lambin, P. A. Thiry, J. J. Pireaux, and R. Caudano, Phys. Scr. **T13**, 150 (1986).

[23]A. S. Barker, Jr., Phys. Rev. **132**, 1474 (1963).

[24]P. Senet, Ph. Lambin, J. P. Vigneron, I. Derycke, and A. A. Lucas, Surf. Sci. **226**, 307 (1990).

[25]H. Schaper and L. L. Van Reijen, Thermochim. Acta **77**, 383 (1984).

[26]P. V. Thomas, V. Ramakrishnan, and V. K. Vaidyan, Thin Solid Films **170**, 35 (1989).

[27]S. J. Wilson and J. D. C. McConnell, J. Solid State Chem. **34**,

315 (1980).

[28]B. R. Frieden, in *Deconvolution with Applications in Spectroscopy,* edited by P. A. Jansson (Academic, New York, 1984), p. 227. The calculations were performed on digitally acquired data using software by Spectrum Square Associates, Inc., 1988.

[29]G. Apai and W. P. McKenna, Langmuir (to be published).

[30]M. Liehr, P. A. Thiry, J. J. Pireaux, and R. Caudano, Phys. Rev. B **33**, 5682 (1986).

[31]Y. T. Chu, J. B. Bates, C. W. White, and G. C. Farlow, J. Appl. Phys. **64**, 3727 (1988).

[32]D. W. Berreman, Phys. Rev. **130**, 2193 (1963); A. J. Maeland, R. Rittenhouse, W. Lahar, and P. V. Romano, Thin Solid Films **21**, 67 (1974); J. Chatelet, H. H. Claassen, D. M. Gruen, I. Sheft, and R. B. Wright, Appl. Spectrosc. **29**, 185 (1975); P. Bruesch, R. Kotz, H. Neff, and L. Pietronero, Phys. Rev. B **29**, 4691 (1984); F. P. Mertens, Surf. Sci. **71**, 161 (1978).

[33]B. G. Frederick, G. Apai, and T. N. Rhodin, J. Electron. Spectrosc. Relat. Phenom. **54/55**, 415 (1990).

[34]J. G. Chen, J. E. Crowell, and J. T. Yates, Jr., J. Chem. Phys. **84**, 5906 (1986).